AEM
Journals.ASM.org

Iron Triggers λSo Prophage Induction and Release of Extracellular DNA in *Shewanella oneidensis* MR-1 Biofilms

Lucas Binnenkade,[a,b] Laura Teichmann,[a] Kai M. Thormann[a,b]

Department of Ecophysiology, Max Planck Institute for terrestrial Microbiology, Marburg, Germany[a]; Institute for Microbiology and Molecular Biology, Justus Liebig University, Giessen, Germany[b]

Prophages are ubiquitous elements within bacterial chromosomes and affect host physiology and ecology in multiple ways. We have previously demonstrated that phage-induced lysis is required for extracellular DNA (eDNA) release and normal biofilm formation in *Shewanella oneidensis* MR-1. Here, we investigated the regulatory mechanisms of prophage λSo spatiotemporal induction in biofilms. To this end, we used a functional fluorescence fusion to monitor λSo activation in various mutant backgrounds and in response to different physiological conditions. λSo induction occurred mainly in a subpopulation of filamentous cells in a strictly RecA-dependent manner, implicating oxidative stress-induced DNA damage as the major trigger. Accordingly, mutants affected in the oxidative stress response (Δ*oxyR*) or iron homeostasis (Δ*fur*) displayed drastically increased levels of phage induction and abnormal biofilm formation, while planktonic cells were not or only marginally affected. To further investigate the role of oxidative stress, we performed a mutant screen and identified two independent amino acid substitutions in OxyR (T104N and L197P) that suppress induction of λSo by hydrogen peroxide (H_2O_2). However, λSo induction was not suppressed in biofilms formed by both mutants, suggesting a minor role of intracellular H_2O_2 in this process. In contrast, addition of iron to biofilms strongly enhanced λSo induction and eDNA release, while both processes were significantly suppressed at low iron levels, strongly indicating that iron is the limiting factor. We conclude that uptake of iron during biofilm formation triggers λSo-mediated lysis of a subpopulation of cells, likely by an increase in iron-mediated DNA damage sensed by RecA.

For the majority of bacteria, the predominant natural lifestyle is assumed to be within surface-associated communities enclosed in self-produced hydrated polymeric matrices, which are commonly referred to as biofilms (1). In comparison to the planktonic lifestyle, biofilm formation provides important advantages, such as elevated concentrations of nutrients in proximity to abiotic surfaces, enhanced genetic exchange, and increased tolerance toward antimicrobial agents, biocides, and host immune responses. Furthermore, living in biofilms protects cells from environmental perturbations causing physical stress, such as drought, UV light, pH gradients, and oxidative stress (2). The integrity and stability of biofilms depends on direct cell-cell and cell-surface interactions and on the extracellular matrix composed of extracellular polymeric substances (EPS), a complex mixture of diverse exopolysaccharides, proteins (including cell appendages such as fimbriae, pili, and flagella), lipids, and extracellular DNA (eDNA) (3). eDNA was initially thought to be mainly residual debris of lysed cells; however, a number of recent studies clearly showed that this compound constitutes an important structural component of the biofilm matrix for many bacterial species (4–10). Additionally, eDNA can serve as a source of phosphorus, carbon, and nitrogen (11, 12), provide a genetic pool for horizontal gene transfer (13), exhibit antimicrobial activity (14), induce antibiotic resistance (14, 15), and facilitate twitching motility-mediated biofilm expansion (16). The origin of eDNA in biofilms has been a focus of numerous studies. So far, three different mechanisms that may allow DNA to be released from bacteria and to accumulate in the biofilm environment have been described: vesiculation (17, 18), secretion (19–21), and cell lysis, which may be the most common source of eDNA in natural environments (5, 6, 22, 23).

As one common mechanism, bacterial cell lysis may occur through induction of prophages, which, either functional or cryptic, often reside stably in bacterial genomes and constitute substantial amounts of bacterial DNA. About 60 to 70% of all sequenced genomes contain prophages (reviewed in reference 24); however, despite this substantial abundance, little is known about their implication in host physiology and ecology. The presence of prophages can provide the host with fitness advantages such as increased growth rates, virulence, and resistance against antibiotics and environmental stress factors (25, 26). A number of studies on both Gram-positive and Gram-negative species have demonstrated the impact of prophages on biofilm development and cell lysis-mediated eDNA release (9, 27–33). However, environmental signals and molecular mechanisms that control prophage induction/excision under biofilm conditions remain elusive for most species. The fact that most prophages in environmental isolates are inducible by DNA-damaging agents (24, 34–37) indicates the existence of common physiological and molecular principles for the control of prophage induction, which might also apply during biofilm growth of the corresponding host bacteria.

We have recently investigated the role of prophage-induced lysis for biofilm formation of *Shewanella oneidensis* MR-1, a Gram-negative facultatively anaerobic gammaproteobacterium. Members of this genus are often recognized for their capacity to

Received 7 May 2014 **Accepted** 13 June 2014
Published ahead of print 20 June 2014
Editor: A. M. Spormann
Address correspondence to Kai M. Thormann, kai.thormann@mikro.bio.uni-giessen.de.
Supplemental material for this article may be found at http://dx.doi.org/10.1128/AEM.01480-14.

doi:10.1128/AEM.01480-14

utilize a broad variety of inorganic and organic compounds as alternative terminal electron acceptors under anaerobic conditions. *S. oneidensis* MR-1 harbors three prophages, LambdaSo (λSo), MuSo1, and MuSo2, of which λSo and MuSo2 are capable of forming infectious particles. Particularly, λSo contributes to cell lysis and eDNA accumulation under biofilm conditions, and accordingly, deletion of the λSo prophage results in strongly impaired biofilm formation of MR-1 (9).

In this study, we aimed to identify the molecular mechanisms and biofilm-specific signals that underlie λSo prophage induction and cell lysis in *S. oneidensis* MR-1 biofilms. To monitor the spatiotemporal induction of prophage λSo under hydrodynamic biofilm conditions at the single-cell level, we constructed a reporter strain harboring a transcriptional fusion of the putative regulator of early λSo gene transcription (Cro) and the yellow fluorescent protein Venus (38). Using that strain, we characterized λSo prophage induction in various genetic backgrounds under different environmental conditions. Our results indicate that colonization of surfaces implies a conflict between high requirements for iron, iron-mediated DNA stress, prophage-induced lysis, and release of biofilm-promoting factors such as eDNA. We show that tight regulation of these partially antagonistic factors is required for successful biofilm formation.

MATERIALS AND METHODS

Growth conditions and media. The bacterial strains and plasmids used in this study are summarized in Table S1 in the supplemental material. *Escherichia coli* and *S. oneidensis* strains were routinely grown as described earlier (9). Biofilms of *S. oneidensis* were cultivated under hydrodynamic or static conditions in LM medium containing 0.5 mM or 15 mM lactate, respectively. $FeCl_2$ (Merck, Darmstadt, Germany) or desferrioxamine (DFO; Sigma-Aldrich, Steinheim, Germany) was added to the medium at a final concentration of 20 μM when indicated. To artificially induce prophage expression and production, cells were either exposed to 1,200 J/m^2 UVC radiation at 254 nm (39) or to mitomycin C (Carl-Roth, Karlsruhe, Germany) at a final concentration of 10 μg ml^{-1}. To induce superoxide generation, planktonic cells were cultivated in LM medium until mid-logarithmic phase and then incubated with paraquat (methyl viologen dichloride hydrate; Sigma-Aldrich, Steinheim, Germany) at a final concentration of 0.2 or 1 mM (40).

Vector and strain constructions. Cloning of DNA fragments was carried out according to standard protocols (41) using appropriate kits (VWR International GmbH, Darmstadt, Germany) and enzymes (New England BioLabs, Frankfurt, Germany; Fermentas, St Leon-Rot, Germany). *S. oneidensis* MR-1 strains constitutively expressing *egfp* or *ecfp* were constructed by using a modified Tn*7* delivery system (9). In-frame deletions into *S. oneidensis* MR-1 were introduced essentially as reported earlier (42) using the suicide vector pNTPS-138-R6K and appropriate primer pairs (see Table S2 in the supplemental material). In-frame deletion mutants were complemented by reinsertion of the corresponding wild-type gene copy into the native locus (see Fig. S1 in the supplemental material). This was also possible for the Δ*recA* mutant, likely enabled by ectopic *recA* expression from the reintegration vector. Genome-integrated transcriptional fusions to *venus* were constructed in a similar manner, using pXVENC-2 as the template for the *venus* coding sequence and pNPTS-138-R6K for markerless insertion downstream of each gene of interest. An optimal ribosomal binding site (AGGAGGNNNNNN) was inserted upstream of each start codon (see Table S1 in the supplemental material). For plasmid-based promoter fusion studies, vector pBBR1-MCS5-TT-RBS-venus was constructed using pBBR1-MCS5-TT and pXVENC-2 as the template. A ribosomal binding site was inserted as elaborated above. Putative promoter regions were cloned into the multiple cloning site, and the resulting plasmid was introduced into *S. oneidensis* MR-1 by conjugation.

Total RNA extraction and RT-PCR. For operon mapping of the putative lysis operon of prophage LambdaSo, total RNA was extracted from *S. oneidensis* MR-1 cells by using a hot-phenol method (43) as described previously (9). To induce transcription of the putative lysis operon, exponentially growing planktonic cultures were incubated with mitomycin C for 2 h, harvested by centrifugation (1 min at 13,000 × *g* and 4°C), and stored in liquid nitrogen. Residual contaminating DNA was removed by using the Turbo DNA-free kit (Applied Biosystems, Darmstadt, Germany) according to the manufacturer's instructions. The quality of the RNA was determined by agarose gel electrophoresis. The extracted total RNA was then applied as the template for random-primed first-strand cDNA synthesis using BioScript reverse transcriptase (RT; Bioline, Luckenwalde, Germany) according to the manufacturer's instructions. Operon mapping was carried out by PCR using the resulting cDNA as the template and appropriate primer pairs bracketing the gaps between the genes that were analyzed. A corresponding total RNA sample taken prior to the reverse transcriptase reaction served as a negative control, and chromosomal DNA served as a positive control. The PCR products were analyzed by 2% agarose gel electrophoresis.

qPCR. *S. oneidensis* MR-1 cultures were grown in LB medium at 30°C to an optical density at 600 nm (OD_{600}) of approximately 1 and exposed to 2 mM H_2O_2 for 15 min. Directly before and after the H_2O_2 treatment, cells were harvested by centrifugation (1 min at 13,000 × *g* and 4°C) and stored immediately in liquid nitrogen. Total RNA extraction and cDNA synthesis were carried out essentially as described for RT-PCR. The cDNA was used as a template for quantitative real-time RT-PCR (qPCR; C1000 Thermal Cycler with the CFX96 Real-Time System; Bio-Rad Laboratories GmbH, Munich, Germany) by using the Sybr green detection system, MicroAmp Optical 96-well reaction plates, and Optica adhesive covers (Applied Biosystems Deutschland GmbH, Darmstadt, Germany). Primers used to determine the expression of the corresponding genes are summarized in Table S2 in the supplemental material. The cycle threshold (C_T) was determined automatically by use of Real-Time CFX Manager 2.1 software (Bio-Rad Laboratories GmbH) after 40 cycles. All C_T values were normalized separately to C_T values obtained for the 16S rRNA and *recA* (SO_3430) genes of each sample. Primer efficiencies and relative expression values were determined according to Pfaffl (44). Each strain was assayed in biological duplicates in two independent experiments.

β-Galactosidase activity in culture supernatants. Extracellular β-galactosidase activity of culture supernatants was determined as previously described (45). Exponentially growing planktonic cultures of *S. oneidensis* MR-1 were incubated with mitomycin C for 3 h. All strains harbored plasmid pME6031-PmotB-lacZ for constitutive cytoplasmic expression of β-galactosidase. To obtain cell-free supernatant, the samples were centrifuged at 2,500 × *g* for 5 min and subsequently filtered (0.2-μm filter). β-Galactosidase assays on supernatants were carried out in reaction tubes at 30°C according to standard protocols (46). The β-galactosidase activity was normalized to the OD_{600} of the culture prior to incubation with mitomycin C. Lysis assays were conducted in triplicate in at least two independent experiments.

Time-lapse analysis of phage-induced lysis. Exponentially growing cultures of strain S2391 were exposed to UVC light and incubated at 30°C with agitation for 3 h. A 4-μl volume of propidium iodide (Sigma-Aldrich, Steinheim, Germany) stock solution (1 mg ml^{-1}) was added on top of agar pads and incubated for several minutes to be completely absorbed into the agar. Subsequently, 4 μl of the cell suspension (OD_{600}, 0.5) was placed on the same agar pad (1% agarose in phosphate-buffered saline [PBS], 137 mM NaCl, 2.7 mM KCl, 6.6 mM Na_2HPO_4, 1.8 mM KH_2PO_4) and analyzed by fluorescence microscopy at 10-min intervals using an Axio Imager.M1 microscope (Zeiss, Wetzlar, Germany) equipped with a Zeiss Plan Apochromate 100×/1.4 differential interference contrast microscopy (DIC) objective.

Determination of cell length. Exponentially growing planktonic cultures of *S. oneidensis* MR-1 were incubated with mitomycin C at a final concentration of 10 μg ml^{-1} for 4 h. All cell suspensions were adjusted to an OD_{600} of 0.5, and 4 μl of each suspension was placed on an agar pad. Image acquisition was carried out by DIC using a Leica DMI6000B microscope equipped with a Leica HCX PlanApo 100×/1.4 to 0.7 oil objective. Cell lengths were determined for at least 800 cells per strain using ImageJ 1.47v software (National Institutes of Health, USA) from duplicates in two independent experiments.

Cultivation of biofilms. (i) Static conditions. Biofilms were cultivated in petri dishes in LM medium as described earlier (9) and harvested by scraping and centrifugation in fresh medium. Cultivation of anaerobically grown biofilms was performed in glass bottles containing glass beads (5-mm diameter; Carl-Roth, Karlsruhe, Germany). The glass beads were completely covered with LM medium containing 15 mM lactate. To remove oxygen from the medium, the bottles were stoppered, sealed, and flushed with nitrogen for several minutes with periodic shaking. Cells were adjusted to an OD_{600} of 0.05 and incubated at room temperature for 24 h. After removal of the supernatant, the cells were harvested by shaking in fresh medium.

(ii) Hydrodynamic conditions. For image acquisition, biofilms were cultivated under hydrodynamic conditions in three-channel flow cells as previously described (9, 47). For eDNA staining, 7-hydroxy-9H-(1,3 dichloro-9,9-dimethylacridin-2-one (DDAO; Invitrogen, Darmstadt, Germany) was added to a final concentration of 4 μM for 1 h prior to microscopy. Microscopic visualization was performed at defined locations close to the inflow. If required, $FeCl_2$ or desferrioxamine mesylate salt was added to the medium reservoir. For protein sampling, biofilm cells were cultivated in 50-ml syringes on glass beads under constant medium flow and harvested as described earlier (48).

CLSM and image acquisition. Microscopic visualization of biofilms and image acquisition was performed using an inverted Leica TCS SP5 confocal laser scanning microscope (CLSM; Leica Microsystems, Wetzlar, Germany) equipped with 10×/0.3. Plan-Neofluar and 63×/1.2 W C-Apochromate objectives. CLSM images were processed using the Imaris software package (Bitplane AG, Zürich, Switzerland) and Adobe Photoshop. Image analysis (e.g., quantification of prophage induction) was conducted using ImageJ 1.47v software, including the LOCI BioFormats plugin. CLSM stacks were split into individual channels (cyan fluorescent protein [Cfp]/Venus/DDAO), and thresholds were adjusted adequately to remove noise. Total signal intensities (limited to the threshold range) were quantified by applying the area-multimeasurement tool on each stack. Cfp signals (constitutively expressed in all cells) were used as a reference to obtain a normalized signal-to-biomass ratio. Biofilm cultivation and measurements were conducted in triplicate in at least two independent experiments.

Chromosome staining. Biofilm cells were harvested in LM medium and washed with PBS. Subsequently, the cells were resuspended in PBS containing 0.1% Triton X and incubated for 10 min on ice. The cells were then sedimented and resuspended in 4% PBS-buffered paraformaldehyde solution containing 10 μg ml^{-1} 4′,6-diamidino-2-phenylindole (DAPI; Sigma-Aldrich, Steinheim, Germany). After 15 min of incubation fluorescence microscopy, image acquisition was carried out using an Axio Imager.M1 microscope equipped with a Zeiss Plan Apochromate 100×/1.4 DIC objective.

Immunoblot analyses. Protein lysates were prepared either from planktonic cells, statically grown biofilm cells, or biofilm cells grown under hydrodynamic conditions on glass beads. Cell suspensions were uniformly adjusted to an OD_{600} of 10 before lysis, and equal volumes of lysate were subsequently subjected to sodium dodecyl sulfate-polyacrylamide gel electrophoresis (SDS-PAGE). For each analysis, one gel was prepared for subsequent Western blotting and one gel was stained with Roti-Blue (Carl Roth, Karlsruhe, Germany) as a loading control (see Fig. S2 in the supplemental material). SDS-PAGE and immunoblot detection of phage λSo was carried out as described previously (9) using polyclonal antibodies raised against SO_2963 and secondary G-horseradish peroxidase-conjugated antibody anti-rabbit immunoglobulin (Thermo Fisher Scientific, Schwerte, Germany). Signals were detected using the SuperSignal West Pico chemiluminescent substrate (Thermo Fisher Scientific) followed by exposition in the Fusion-SL chemiluminescence imager (Peqlab, Erlangen, Germany). Representative immunoblot patterns are presented here, but similar patterns were obtained from at least two biological replicates.

Isolation of H_2O_2-resistant mutants. For the isolation and identification of an *oxyR* mutation that provides increased resistance against H_2O_2 in *S. oneidensis* MR-1, we used an approach similar to that described earlier for *Xanthomonas campestris* (49, 50). To avoid selection of mutations in prophage genomes that would reduce induction and/or lysis, we used the prophage-deficient strain S1419 as the template. In total, approximately 1.5×10^{10} cells in mid-exponential phase were transferred to LB agar plates (1.5×10^8 cells/plate) containing 2 mM H_2O_2 (Carl-Roth, Karlsruhe, Germany). To verify that mutants retain resistance after nonselective growth, single colonies were cultivated overnight in plain LB and reinoculated in LB medium containing 10 mM H_2O_2. Mutated *oxyR* regions were sequenced, cloned into pNPTS-128-R6K, and reintroduced into strain S2991 and strain S2391 by markerless in-frame insertion. Resistance was confirmed by cultivation in LB containing 10 mM H_2O_2.

RESULTS

λSo prophage-mediated lysis is required for normal biofilm formation. In a previous study, we demonstrated that an *S. oneidensis* MR-1 mutant devoid of prophage λSo was unable to cover the surface during later phases of biofilm development (24 h) and to form distinct three-dimensional structures (9). To further determine whether phage-mediated cell lysis is the major biofilm-promoting factor of λSo (and not additional factors encoded by the prophage), we deleted the prophage's putative lysis operon (SO_2966-SO_2974), which was identified by bioinformatic analyses and RT-PCR (see Fig. S3A and B in the supplemental material). The MR-1 mutant lacking this operon displayed a phenotype undistinguishable from that of a mutant lacking the whole λSo prophage with respect to cell lysis (as determined by extracellular β-galactosidase activity after prophage induction of strains constitutively expressing β-galactosidase) and biofilm formation under hydrodynamic conditions (see Fig. S3C to E in the supplemental material). We concluded that cell lysis is the major biofilm-promoting factor of the λSo prophage.

Biofilm conditions trigger λSo prophage induction. To generate strains that allow monitoring of λSo induction at a single-cell level, the coding sequence for *venus* was inserted into the prophage λSo genome downstream of SO_2989 (encoding the putative transcriptional regulator Cro) by homologous recombination, resulting in strain Pλ*cro*::*venus* (see Fig. S4 in the supplemental material). Additionally, the strain was provided with constitutively expressed *ecfp* at the Tn*7* site for confocal laser scanning microscopy analyses. Analogous strains harboring transcriptional fusions to the putative λSo lysis promoter ($P_{R'}$, upstream of gene SO_2974) and putative tail protein L (downstream of SO_2949) were similarly generated. Results obtained for these strains were congruent with those obtained for strain Pλ*cro*::*venus*. Thus, within this study we will exclusively focus on strain Pλ*cro*::*venus*.

To demonstrate that prophage induction in strain Pλ*cro*::*venus* correlates with Venus fluorescence, cultures were exposed to UVC light or mitomycin C and analyzed by fluorescence microscopy. Approximately 2 h after exposure, a significant fraction of cells started to display filamentous growth and Venus fluorescence. To further determine whether phage induction is ultimately followed by cell lysis, a mitomycin C-treated culture of strain Pλ*cro*::*venus*

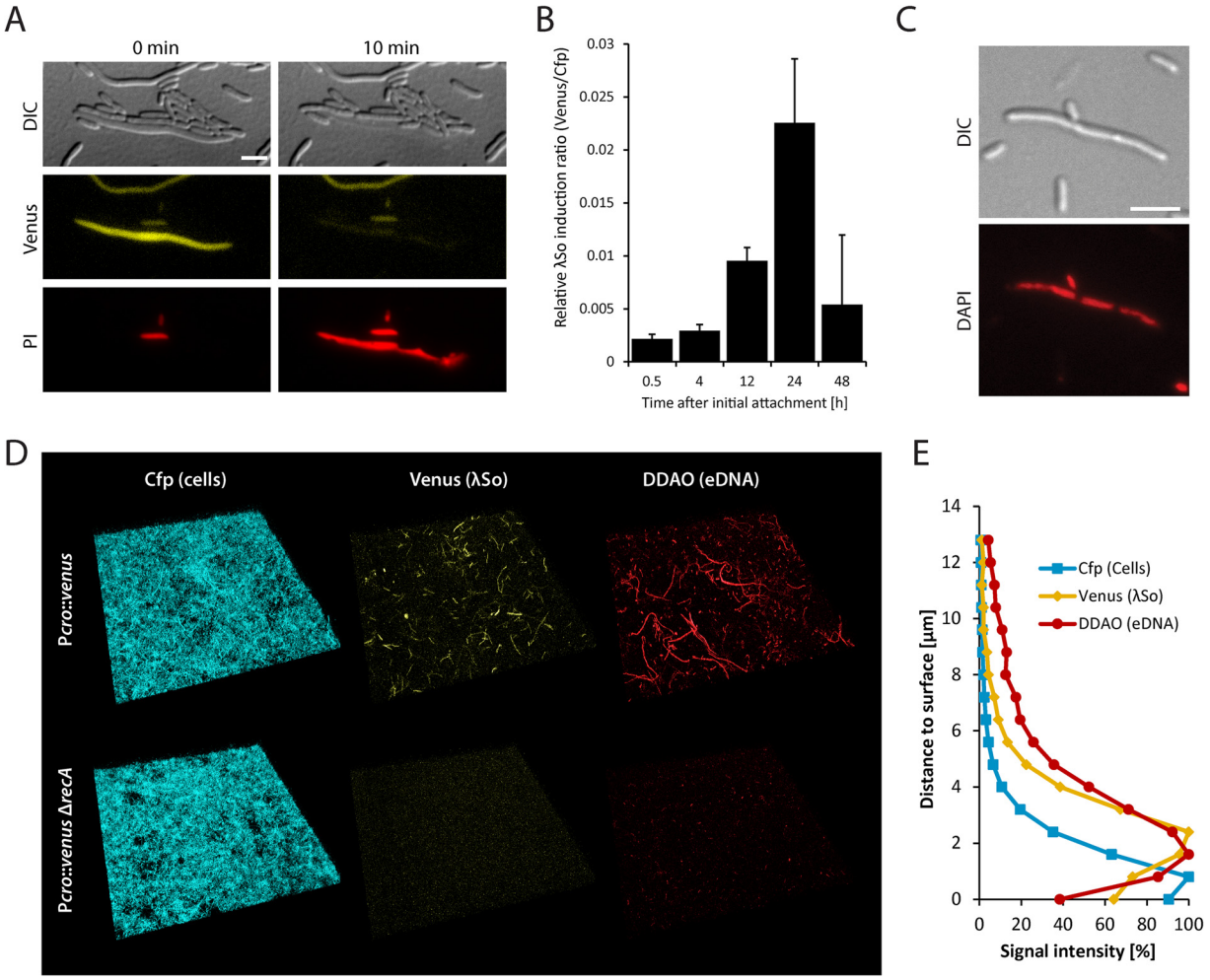

FIG 1 Determination of λSo prophage induction and eDNA release. (A) Visualization of λSo prophage-induced cell lysis by differential interference contrast microscopy (DIC) and detection of Venus fluorescence and propidium iodide (PI) fluorescence in cells of strain P*λcro*::*venus* after UV exposure. Scale bar, 5 μm. (B) Relative λSo induction over time in biofilms formed by strain P*λcro*::*venus* under hydrodynamic conditions in flow cells. Total Venus signal intensities from CLSM images were normalized to total Cfp signal intensities to obtain an induction-to-biomass ratio. Black bars represent the mean values, with standard deviations displayed as error bars, obtained from two independent experiments conducted each in triplicat. (C) DAPI staining of nucleoids (red) in filamentous biofilm cells of *S. oneidensis* MR-1. Scale bar, 5 μm. (D) Projections of CLSM images displaying the induction of prophage λSo (Venus fluorescence) and eDNA (stained with DDAO) in biofilms formed by the Cfp-tagged strains P*λcro*::*venus* and P*λcro*::*venus* Δ*recA* under hydrodynamic conditions in flow cells 24 h after the initial attachment. The lateral edge of each micrograph is 250 μm. (E) Distribution of total Cfp, Venus, and DDAO signal intensities (as percentage of maximal intensity of each channel) over the *z* axis (distance to surface) of CLSM images of biofilms formed by strain P*λcro*::*venus* under hydrodynamic conditions in flow cells 24 h after the initial attachment. Relative signal intensities are derived from the mean pixel values of triplicates in a representative experiment.

was immobilized on a propidium iodide-containing agar pad and analyzed by time-lapse microscopy (Fig. 1A). Single cells that were exhibiting a simultaneous loss of turgor pressure and Venus fluorescence in concert with sudden appearance of propidium iodide fluorescence, strongly indicative of cell lysis, were observed. The time interval between induction and lysis was highly variable, and induction did not necessarily result in complete lysis of the MR-1 population.

Based on these results, we concluded strain P*λcro*::*venus* to be a useful tool to monitor spatiotemporal induction of the prophage λSo lytic cycle. To this end, biofilms of strain P*λcro*::*venus* were cultivated under hydrodynamic conditions and visualized by CLSM over 48 h. Induction of prophage λSo peaked at around 24 h after initial attachment at the developmental transition phase prior to extensive three-dimensional growth (Fig. 1B). While only single cells produced Venus during the first hours at a degree comparable to spontaneous induction in planktonic cultures, a large subpopulation of mainly filamentous cells displayed increased fluorescence after 24 h. When *S. oneidensis* MR-1 biofilms were treated with cell-impermeable DNA stain DDAO, similar stringlike structures appeared, a phenotype that has already been observed in previous studies (9). However, fluorescence signals of both structures did not colocalize, strongly implicating that the DDAO-stained stringlike structures represent dead cells after λSo-induced lysis. DAPI staining of filamentous cells isolated from biofilms revealed the presence of multiple chromosomes, indicating that the cell length of filamentous cells positively correlates with the amount of DNA per cell body (Fig. 1C). Analysis of

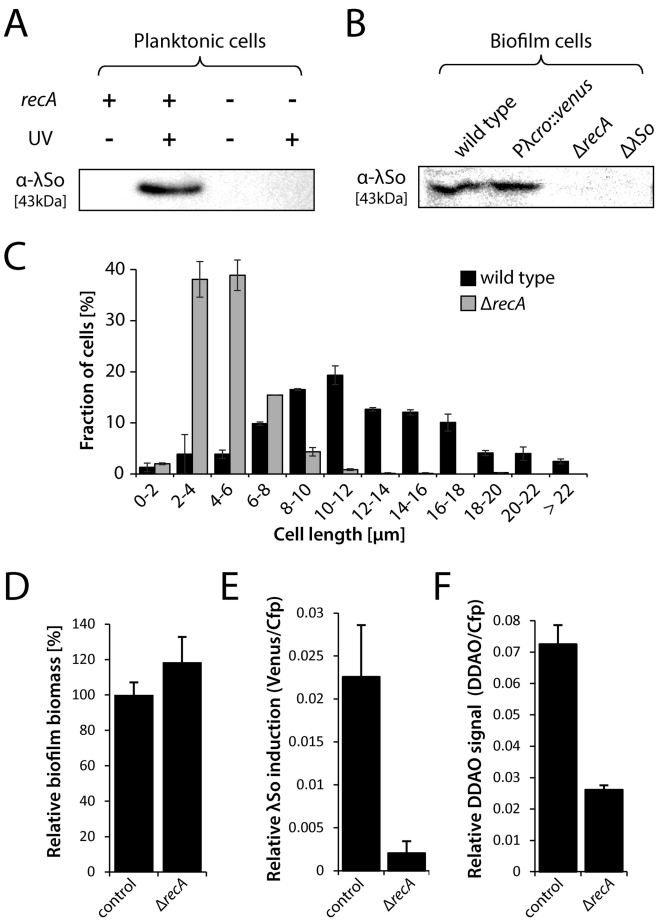

FIG 2 Induction of prophage λSo and filamentous cell growth in Δ*recA* deletion mutants. (A) λSo production in planktonic cells of the wild type (*recA* +) and Δ*recA* deletion mutants (*recA* −) after UV exposure (+) or without UV exposure (−). Whole-cell lysates were separated by SDS-PAGE followed by Western immunodetection of major capsid protein SO_2963. Sample normalization was achieved by adjusting cell suspensions to the same OD_{600} and analysis of stained SDS-PAGE gels (see Fig. S2 in the supplemental material). Representative immunoblot patterns from at least two independent experiments are presented. (B) Production of phage λSo in biofilm cells of the wild type, strain Pλ*cro*::*venus*, a Δ*recA* deletion mutant, and the Δλ*So* deletion mutant of prophage λSo. Biofilms were cultivated under static conditions in petri dishes for 24 h, and biofilm cells were harvested by scraping. Whole-cell lysates were separated by SDS-PAGE followed by immunoblot analysis of major capsid protein SO_2963. Sample normalization was achieved by adjusting cell suspensions to the same OD_{600} and analysis of stained SDS-PAGE gels (see Fig. S2 in the supplemental material). Representative immunoblot patterns from at least two independent experiments are presented. (C) Cell length distribution of planktonic wild-type and Δ*recA* deletion mutant cells of *S. oneidensis* MR-1 in response to mitomycin C. Black and gray bars (*S. oneidensis* MR-1 wild type and Δ*recA* mutant, respectively) represent the mean values, with standard deviations displayed as error bars, of the percentages of each cell length obtained from two independent experiments conducted each in duplicate with at least 800 cells per strain. (D) Relative biomass (total Cfp signal compared to the wild type) of 24-h-old biofilms formed by strain Pλ*cro*::*venus* and Pλ*cro*::*venus* Δ*recA* under hydrodynamic conditions in flow cells. Bars represent the means of Cfp values (in percentages), with standard deviations displayed as error bars, obtained from two independent experiments conducted at least in duplicate. (E) Relative λSo induction of 24-h-old biofilms formed by strains Pλ*cro*::*venus* and Pλ*cro*::*venus* Δ*recA* under hydrodynamic conditions in flow cells. Total Venus signal intensities from CLSM images were normalized to total Cfp signal intensities to obtain an induction-to-biomass ratio. Black bars represent the mean values, with standard deviations displayed as error bars, obtained from two independent experiments conducted each in duplicate. (F) eDNA levels as a measure of relative DDAO fluorescence in 24-h-old biofilms formed by strain Pλ*cro*::*venus* and Pλ*cro*::*venus* Δ*recA* under hydrodynamic conditions in flow cells. Total DDAO signal intensities from CLSM files were normalized to total Cfp signal intensities to obtain an eDNA-to-biomass ratio. Black bars represent the mean values, with standard deviations displayed as error bars, obtained from two independent experiments conducted at least in duplicate.

the distribution of cells exhibiting Venus fluorescence along the *z* axis in 24-h-old biofilms revealed that signal intensities were strongest in a distance of approximately 1.5 to 2.5 μm to the glass surface at the top of the yet-thin cell layer, whereas the basal Cfp signal displayed its strongest fluorescence at a distance of 0 to 0.8 μm, representing the bottom layers of the biofilm. DDAO signals showed a pattern similar to that of Venus, indicating that induction of prophage λSo and cell lysis predominantly occur within the upper layers of the biofilm during this developmental stage. Along the *x* and *y* axes, signals were evenly distributed, except in densely packed micro- or macrocolonies, which mostly lacked *venus*-expressing filamentous cells or stringlike eDNA structures.

RecA controls λSo prophage induction and eDNA release in *S. oneidensis* MR-1 biofilms. Since induction of the lytic cycle in Lambda-like phages is thought to occur via the RecA-mediated autocleavage of phage repressor cI in response to DNA-damaging agents, we hypothesized that prophage λSo induction might similarly be RecA dependent. Thus, we generated a *recA* in-frame deletion mutant in strain Pλ*cro*::*venus* and examined the response of planktonic cultures to UV exposure. Fluorescence microscopy (data not shown) and immunoblot analysis verified that deletion of *recA* suppressed λSo induction and production (Fig. 2A). Furthermore, filamentous growth in response to DNA-damaging agents was largely suppressed by deletion of *recA* in *S. oneidensis* MR-1 (Fig. 2C).

To determine whether induction of prophage λSo in biofilms is also a RecA-dependent process, Pλ*cro*::*venus* Δ*recA* biofilms were grown under hydrodynamic conditions and analyzed by CLSM. No fluorescence of Venus above the background level was observed in any of the biofilm developmental stages (Fig. 1D and 2E). Accordingly, phage production in biofilm cells was suppressed, as confirmed by immunoblot analysis (Fig. 2B). Unexpectedly, the total biomass of Pλ*cro*::*venus* Δ*recA* biofilms (Cfp signal) was slightly increased in comparison to the wild type and did not phenocopy the ΔλSo strain (Fig. 2D; see also Fig. S3E in the supplemental material), possibly due to pleiotropic effects of the Δ*recA* deletion. eDNA staining of 24-h-old biofilms formed by Pλ*cro*::*venus* Δ*recA* demonstrated that the relative signal intensity of DDAO was reduced at least 2.8-fold in comparison to strain Pλ*cro*::*venus*, indicating that deletion of *recA* suppressed λSo-mediated eDNA release (Fig. 2F). In addition, significantly fewer stringlike structures were observed after DDAO staining of eDNA. From these data, we concluded that RecA-controlled induction of prophage λSo mediates cell lysis and eDNA release in a subpopulation of filamentous cells in *S. oneidensis* MR-1 biofilms, mainly at the developmental transition phase prior to extensive three-dimensional growth.

Regulation by OxyR and Fur affects λSo prophage induction. In a previous study, we demonstrated that early surface-associated growth induces the expression of genes belonging to the putative OxyR (oxidative stress defense regulator) and Fur (ferric uptake regulator) regulons in *S. oneidensis* MR-1 (48). Based on these

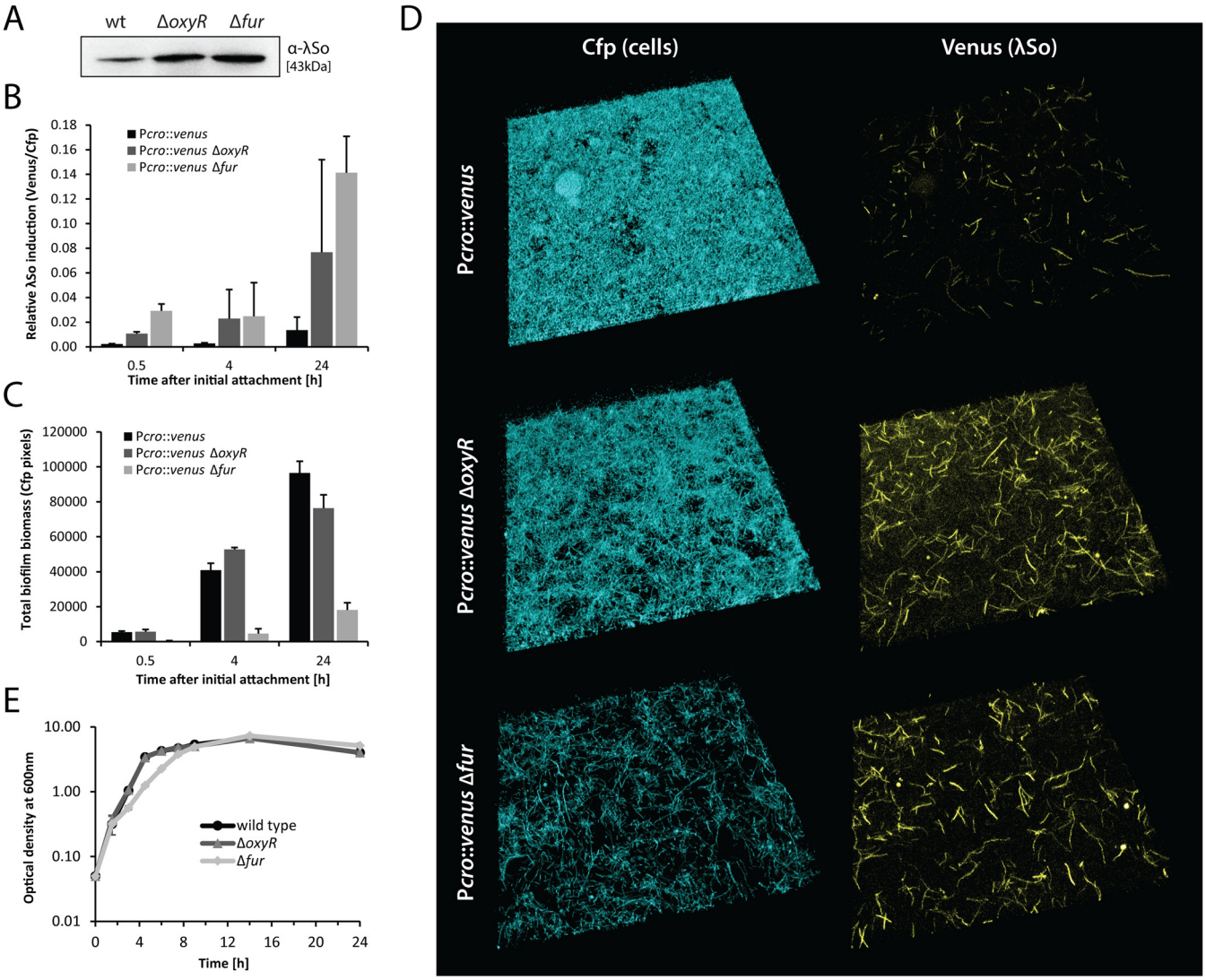

FIG 3 Regulation by OxyR and Fur affects λSo prophage induction and biofilm development. (A) Detection of phage λSo by immunoblot analysis in biofilms formed by the wild type, the Δ*oxyR* deletion mutant, and the Δ*fur* deletion mutant under static conditions in petri dishes. Sample normalization was achieved by adjusting cell suspensions to the same OD_{600} and analysis of stained SDS-PAGE gels (see Fig. S2 in the supplemental material). Representative immunoblot patterns from at least two independent experiments are presented. (B) Relative induction of λSo prophage over time in biofilms formed by strains Pλ*cro*::*venus* (black), Pλ*cro*::*venus* Δ*oxyR* (dark gray), and Pλ*cro*::*venus* Δ*fur* (light gray) under hydrodynamic conditions in flow cells. Bars represent the mean values of Venus/Cfp ratios, with standard deviations displayed as error bars, obtained from two independent experiments conducted at least in duplicate. (C) Accumulation of biofilm biomass (Cfp signal) over time of strains Pλ*cro*::*venus*, Pλ*cro*::*venus* Δ*oxyR*, and Pλ*cro*::*venus* Δ*fur* under hydrodynamic conditions in flow cells. Bars represent the mean values of total Cfp pixel values, with standard deviations displayed as error bars, obtained from two independent experiments conducted at least in duplicate. (D) CLSM images of 24-h-old biofilms formed by strains Pλ*cro*::*venus*, Pλ*cro*::*venus* Δ*oxyR*, and Pλ*cro*::*venus* Δ*fur* under hydrodynamic conditions in flow cells. Cfp fluorescence represents all cells, and Venus fluorescence indicates λSo prophage induction. (E) Planktonic growth of *S. oneidensis* MR-1 wild type, the Δ*oxyR* deletion mutant, and the Δ*fur* deletion mutant in LB medium under aerobic conditions. Growth curves are derived from one representative experiment conducted in triplicate. Error bars represent standard deviations.

observations, we hypothesized that iron-mediated oxidative stress might generate DNA damage under biofilm conditions, which ultimately induces λSo via RecA.

To investigate the role of oxidative stress and intracellular iron levels for the induction of prophage λSo in *S. oneidensis* MR-1 biofilms, we generated in-frame deletion mutants of *oxyR* and *fur*. A recent study demonstrated that OxyR in *S. oneidensis* MR-1 is analogous to OxyR in *Escherichia coli* and mediates the response to hydrogen peroxide (H_2O_2)-induced stress by acting both as an activator and as a repressor of defense genes (51). Hence, *oxyR* mutants were expected to exhibit a partially impaired response to oxidative stress. Deletion of *fur* should result in an increase in intracellular iron levels, since Fur acts as a repressor of iron uptake genes in *S. oneidensis* MR-1 (52).

Immunoblot analysis of λSo in Δ*oxyR* and Δ*fur* biofilm cells (static conditions) indicated increased levels of λSo production in both mutants compared to the wild type (Fig. 3A). To further investigate the impact of both mutations on λSo prophage induction during biofilm formation under hydrodynamic conditions, both mutations were introduced into strain Pλ*cro*::*venus*. In both

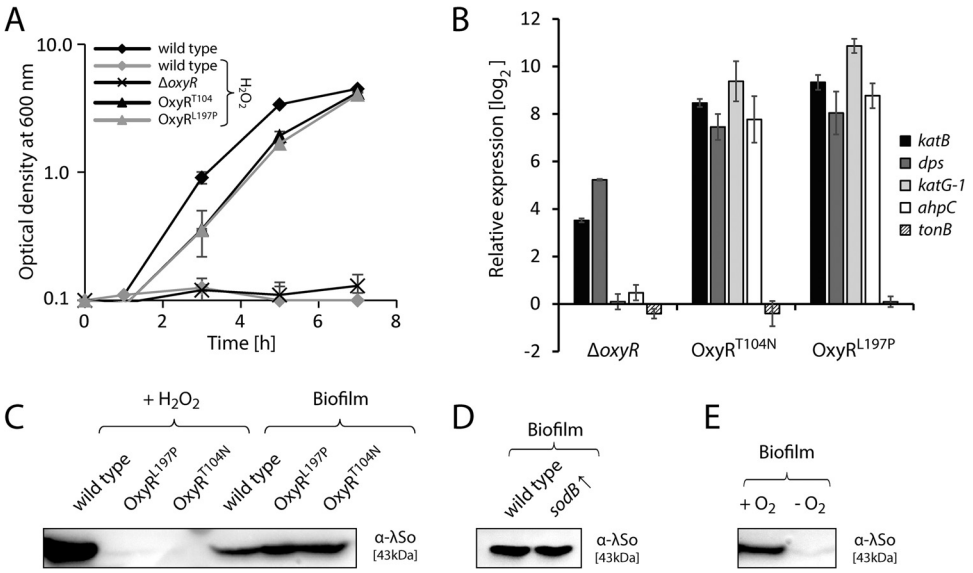

FIG 4 Induction of prophage λSo in biofilms is independent of hydrogen peroxide and superoxide. (A) Planktonic growth under aerobic conditions in LB medium containing 10 mM H_2O_2 of the *S. oneidensis* MR-1 wild type, the Δ*oxyR* deletion mutant, and mutant strains that harbor single amino acid substitution T104N or L197P in OxyR (OxyR^{T104N} and OxyR^{L197P}). As a reference, the growth curve of the wild type in the absence of H_2O_2 is also presented. Growth curves are derived from a representative experiment conducted in triplicate. Error bars represent standard deviations. (B) Expression, relative to the wild type, of *katB* (SO_1070), *dps* (SO_1158), *ahpC* (SO_0958), *katG1* (SO_0725), and *tonB* (SO_3670) in the Δ*oxyR* and the OxyR^{T104N} and OxyR^{L197P} mutant strains, determined by quantitative real-time RT-PCR. Bars represent the mean values of two independent experiments, each normalized to the 16S rRNA and *recA* housekeeping genes. Standard deviations are displayed as error bars. (C) Left three lanes (+ H_2O_2), immunoblot analysis of phage λSo production in planktonic cells of the wild type and the OxyR^{T104N} and OxyR^{L197P} mutants. Cells were cultivated in LB medium until mid-exponential phase and subjected to 2 mM H_2O_2 for 2 h. Right three lanes (Biofilm), immunoblot analysis of phage λSo production in biofilm cells of the wild type and the two OxyR mutants. Cells were harvested from 24-h-old biofilms formed on glass beads under hydrodynamic conditions. Sample normalization was achieved by adjusting cell suspensions to the same OD_{600} and analysis of stained SDS-PAGE gels (see Fig. S2 in the supplemental material). Representative immunoblot patterns from at least two independent experiments are presented. (D) Immunoblot analysis of phage λSo production in wild-type biofilm cells harboring plasmid pBBR1-TT-Ptac-MSC5-*sodB* for constitutive overexpression of superoxide dismutase gene *sodB*. Cells were harvested from 24-h-old biofilms formed on glass beads under hydrodynamic conditions. Sample normalization was achieved by adjusting cell suspensions to the same OD_{600} and analysis of stained SDS-PAGE gels (see Fig. S2 in the supplemental material). Representative immunoblot patterns from at least two independent experiments are presented. (E) Immunoblot analysis of phage λSo production in wild-type cells harvested from biofilms formed under oxic conditions (+ O_2) on glass beads (constant medium flow) and cells harvested from biofilms formed under anoxic conditions (− O_2; N_2 headspace) on glass beads (static conditions). Sample normalization was achieved by adjusting cell suspensions to the same OD_{600} and analysis of stained SDS-PAGE gels (see Fig. S2 in the supplemental material). Representative immunoblot patterns from at least two independent experiments are presented.

mutants, relative induction of λSo was severely increased throughout biofilm development during the first 24 h (approximately 6-fold for the Δ*oxyR* mutant and 12-fold for the Δ*fur* mutant [Fig. 3B]). Δ*oxyR* mutants produced loosely packed and unstructured biofilms mostly consisting of filamentous cells; however, the total biofilm biomass was only slightly reduced 24 h after the initial attachment (Fig. 3C and D). The Δ*fur* mutant was strongly defective in biofilm formation during all developmental phases tested, and the accumulated biomass ranged between 10 and 20% of that of the wild-type biofilms (Fig. 3C). Twenty-four-hour-old biofilms almost exclusively consisted of randomly oriented and loosely packed filamentous cells (Fig. 3D). Δ*fur* mutants were also unable to produce densely packed macrocolonies under the conditions tested. Notably, under planktonic growth conditions in LB medium, the Δ*oxyR* mutant exhibited no growth defect and the Δ*fur* mutant had only slightly reduced growth rates in late exponential phase (Fig. 3E). Our results indicate that surface-associated growth of *S. oneidensis* MR-1 strongly requires an inducible defense against oxidative stress and tight control of iron uptake. Deregulation of either process triggers λSo prophage induction to abnormal levels, resulting in defective biofilm formation.

λSo induction in biofilms cannot be suppressed by an increase in cellular H_2O_2 turnover. Since deregulation of the oxidative stress response in the Δ*oxyR* mutant and elevated uptake of iron in the Δ*fur* mutant both increased the level of λSo prophage induction, the question arose as to whether elevated H_2O_2 levels might occur under biofilm conditions, resulting in Fenton-mediated DNA damage and λSo prophage induction. Accordingly, reduction or elimination of intracellular H_2O_2 by an increase in cellular turnover of H_2O_2 would be expected to indirectly reduce, or even suppress, RecA-mediated induction of prophage λSo. To explore the role of H_2O_2, we performed a mutant screening for the isolation of H_2O_2-resistant clones that possibly possess a constitutively active response to oxidative stress.

Of four isolated resistant clones, sequencing of *oxyR* genes revealed a single point mutation causing a T104N amino acid substitution in 3 isolates and another single point mutation causing an L197P substitution in 1 isolate (see Fig. S5A in the supplemental material). Reintroduction of both point mutations into the wild-type background revealed that both mutations individually provide *S. oneidensis* MR-1 with a strongly increased resistance (>20-fold) against H_2O_2 compared to the wild type and the Δ*oxyR* mutant (Fig. 4A). In plain LB medium, the mutants

showed slightly reduced growth rates compared to the wild type (see Fig. S5B in the supplemental material). Quantitative real-time RT-PCR was performed to better understand the effects of both amino acid substitutions in OxyR on the expression of potential target genes in the absence and the presence of H_2O_2. In both mutants ($OxyR^{T104N}$ and $OxyR^{L197P}$), the expression of *katB* (SO_1070), *dps* (SO_1158), *ahpC* (SO_0958), and *katG1* (SO_0725) was strongly induced, by factors ranging from 170 (*dps* in $OxyR^{T104N}$) to 1,860 (*katG1* in $OxyR^{L197P}$), compared to the wild type, regardless of the presence or absence of H_2O_2 (Fig. 4B; see also Fig. S5C in the supplemental material). Transcript levels of *tonB* (SO_3670) were also examined to determine whether deletion of *oxyR* or expression of the OxyR variants $OxyR^{T104N}$ and $OxyR^{L197P}$ influences the expression of the Fur regulon. However, no differential expression of *tonB* was observed in the absence of H_2O_2 and only slight downregulation in the OxyR variants occurred in the presence of H_2O_2 (see Fig. S5C in the supplemental material). We conclude that resistance against H_2O_2 in strains expressing the OxyR variants $OxyR^{T104N}$ and $OxyR^{L197P}$ is conferred by constitutive overexpression of H_2O_2 defense genes and an increase in H_2O_2 turnover.

To determine whether expression of the OxyR variant $OxyR^{T104N}$ or $OxyR^{L197P}$ suppresses λSo induction by H_2O_2, we performed immunoblot analysis on planktonic cultures treated with 2 mM H_2O_2. Our results demonstrate that λSo production was strongly reduced in both mutants compared to that of the wild type (Fig. 4C). Accordingly, cell morphologies of the mutants were unaffected by H_2O_2, while the wild type displayed filamentous cell morphologies (see Fig. S5D in the supplemental material).

To finally determine whether induction of prophage λSo is similarly suppressed under biofilm conditions, both *oxyR* mutations were individually introduced into strain Pλ*cro*::*venus*. Surprisingly, λSo induction levels and biofilm morphologies of the mutants were indistinguishable from those of the wild type, as indicated by CLSM analyses (data not shown). Immunoblot analysis of phage λSo in biofilm cells cultivated under hydrodynamic conditions confirmed similar levels of phage λSo production in both mutants and the wild type, indicating that H_2O_2 is not a limiting factor for λSo induction in *S. oneidensis* MR-1 biofilms.

In addition to H_2O_2, we were intrigued by the question of whether elevated superoxide levels might influence λSo activation under biofilm conditions. However, addition of paraquat did not stimulate λSo production in planktonic cells, and overexpression of the Fe/Mn superoxide dismutase *sodB* gene (SO_2881) in biofilm cells did not suppress λSo production, indicating that superoxide has a rather minor role, if any, in λSo induction in *S. oneidensis* MR-1 biofilms (Fig. 4D; see also Fig. S6 in the supplemental material). We also tested a range of molecules (glutathione, ascorbic acid, N-acetyl-cysteine, L-proline, and L-cysteine) that might act as antioxidants and have previously been shown to suppress cellular oxidative stress, but none had any significant effect on phage induction during biofilm formation (data not shown). In contrast, cultivation of biofilms under anoxic conditions strongly decreased the level of λSo production in comparison to those grown aerobically, indicating that dioxygen plays an important role in the induction of λSo under hydrodynamic biofilm conditions (Fig. 4E). However, it has to be noted that the setup used for the cultivation of anaerobic biofilms differs considerably from that used for aerobic biofilms and therefore represents only a limited control.

From this set of experiments, we conclude that an inducible defense against reactive oxygen species is required for normal biofilm formation; however, neither increased H_2O_2 nor increased superoxide levels seem to represent a biofilm-specific stimulus of prophage λSo.

Availability of soluble iron controls the timing and level of λSo prophage induction and eDNA release. We previously demonstrated that in *S. oneidensis* MR-1, genes of the Fur (ferric uptake regulator) regulon were strongly induced upon surface contact, indicating a high demand of iron during this phase. Addition of Fe^{2+} to *S. oneidensis* MR-1 biofilms cultivated under hydrodynamic conditions significantly stimulated biofilm formation, while planktonic growth was not affected (48). Increased intracellular levels of free iron in concert with aerobic respiration have often been suggested to result in oxidative stress and DNA damage, a well-known stimulus for the RecA-mediated SOS response (for reviews, see references 53, 54, and 55). We thus hypothesized that iron might act as an indirect stimulus for λSo phage induction and eDNA release in *S. oneidensis* MR-1 biofilms. To analyze this, biofilms of strain Pλ*cro*::*venus* were cultivated in the presence of 20 μM Fe^{2+}. After 12 h of incubation, Venus fluorescence as a measure of λSo prophage induction was increased in comparison to that of biofilms without additional iron but decreased after 24 h after initial attachment, indicating that addition of iron stimulated an earlier λSo induction (Fig. 5B). DDAO staining of 24-h-old biofilms revealed drastically increased levels of eDNA (9.5-fold) in comparison to biofilms grown without additional iron (Fig. 5A and C). The eDNA appeared as densely packed stringlike structures, probably representing filamentous multinucleated cell bodies that pervaded the entire biofilm except the area of microcolonies (Fig. 5A). In contrast, addition of desferrioxamine, a chelating agent for ferric and ferrous iron (56), reduced the relative signal intensities of both Venus and DDAO, indicating that decreasing the levels of available iron inhibits λSo phage induction and eDNA release. Accordingly, the presence of DDAO-stained stringlike structures was largely diminished. Suppression of λSo production by desferrioxamine in hydrodynamically grown biofilms was additionally verified by immunoblot analysis (Fig. 5D). Notably, the observed effect of iron on λSo induction appeared to be biofilm specific, since addition of Fe^{2+} to cells grown under planktonic conditions did not have any effect on λSo production (Fig. 5E).

The effect of iron was additionally investigated by immunoblot analysis in wild-type and Δ*fur* biofilms grown under static conditions. In both strains, addition of ferrous iron increased the level of λSo production compared to the untreated controls. Moreover, addition of iron to Δ*fur* biofilms had an additive effect, resulting in strongly increased levels of λSo production (Fig. 5F and G). These results suggested that the level of intracellular iron positively correlates with the degree of λSo production in *S. oneidensis* MR-1 biofilms. Notably, addition of Fe^{2+} to biofilms formed by the $OxyR^{T104N}$ and $OxyR^{L197P}$ mutant strains also strongly increased the level of λSo production in comparison to the untreated controls, further indicating that iron and not H_2O_2 is the predominant factor for λSo induction in *S. oneidensis* biofilms (see Fig. S7 in the supplemental material).

From this set of experiments, we concluded that addition of Fe^{2+} to biofilms of *S. oneidensis* MR-1 stimulates λSo prophage

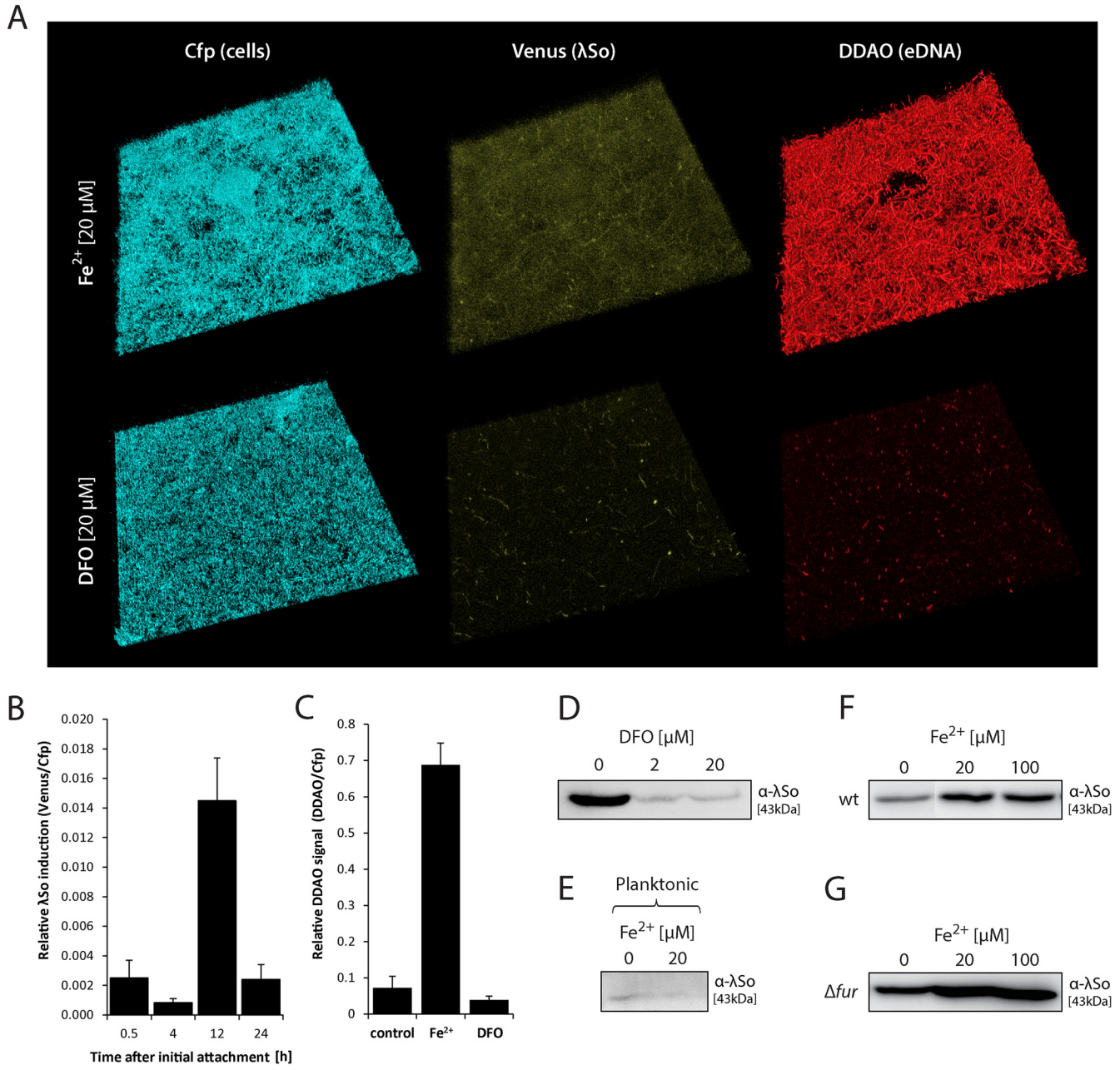

FIG 5 Iron controls the level and timing of λSo prophage induction and eDNA release. (A) CLSM image projections of 24-h-old biofilms formed by strain P*λcro*::*venus* under hydrodynamic conditions in flow cells in the presence of 20 μM $FeCl_2$ (Fe^{2+}) or 20 μM iron chelator desferrioxamine (DFO). Cfp fluorescence represents all cells, and Venus fluorescence indicates λSo prophage induction. The biofilms were stained with DDAO to visualize eDNA. The lateral edge of each micrograph is 250 μm. (B) Relative induction of λSo prophage over time in biofilms formed by strain P*λcro*::*venus* under hydrodynamic conditions in flow cells in the presence of 20 μM Fe^{2+}. Total Venus signal intensities from CLSM images were normalized to total Cfp signal intensities to obtain an induction-to-biomass ratio. Black bars represent the mean values with standard deviations displayed as error bars, obtained from two independent experiments conducted at least in duplicates. (C) eDNA levels as a measure of relative DDAO fluorescence in biofilms formed under hydrodynamic conditions in flow cells in the presence of 20 μM Fe^{2+} or 20 μM iron chelator DFO. Total DDAO signal intensities from CLSM files were normalized to total Cfp signal intensities to obtain an eDNA-to-biomass ratio. Black bars represent the mean values, with standard deviations displayed as error bars, obtained from two independent experiments conducted at least in duplicate. (D) Detection of phage λSo by immunoblot analysis in biofilms formed under hydrodynamic conditions on glass beads in the presence or absence of DFO. Sample normalization was achieved by adjusting cell suspensions to the same OD_{600} and analysis of stained SDS-PAGE gels (see Fig. S2 in the supplemental material). Representative immunoblot patterns from at least two independent experiments are presented. (E) Detection of phage λSo by immunoblot analysis in wild-type cells cultivated under planktonic growth conditions in the absence or presence of 20 μM Fe^{2+}. The cells were harvested during logarithmic growth phase. Sample normalization was achieved by adjusting cell suspensions to the same OD_{600} and analysis of stained SDS-PAGE gels (see Fig. S2 in the supplemental material). Representative immunoblot patterns from at least two independent experiments are presented. (F and G) Detection of phage λSo by immunoblot analysis in biofilms formed by the wild type (F) and the Δ*fur* deletion mutant (G) under static conditions in petri dishes in the presence of 20 μM and 100 μM Fe^{2+}. Cell lysates of biofilm cells were subjected by SDS-PAGE followed by immunoblot analysis of major capsid protein SO_2963. Sample normalization was achieved by adjusting cell suspensions to the same OD_{600} and analysis of stained SDS-PAGE gels (see Fig. S2 in the supplemental material). Representative immunoblot patterns from at least two independent experiments are presented.

induction and enhances the level of eDNA release, likely by an increase in oxidative stress and DNA damage. This hypothesis was further supported by monitoring *dps* (SO_1158) promoter activity during biofilm formation (see Fig. S8A in the supplemental material). Dps is predicted to be a ferritinlike protein that binds and oxidizes Fe^{2+} to protect DNA against oxidative damage (57, 58). While *dps* appeared to be actively expressed in almost all cells during the early phases of biofilm formation, reporter activity occurred solely in filamentous cells during later phases. In contrast, *dps* expression in planktonic cells was mostly below the detection limit of the reporter system.

DISCUSSION

The ubiquitous presence of prophages in bacterial genomes has numerous implications with respect to host physiology and ecology, which we are just beginning to understand. Since biofilms are the predominant form of bacterial existence, the question arises as to what extent prophages impact biofilm formation. For different species, including *S. oneidensis* MR-1, it has been suggested that prophage-induced lysis promotes biofilm formation, e.g., by the release of matrix components such as eDNA (9, 32, 33). To our knowledge, this is the first study in which high-resolution CLSM was utilized to elaborate the spatiotemporal induction of a prophage during biofilm formation at the single-cell level and to visualize the heterogeneity of this process within the biofilm community. Our results strongly suggest that in *S. oneidensis* MR-1, λSo induction occurs mainly in upper biofilm layers in a subpopulation of filamentous cells. We show that induction and, ultimately, cell lysis and eDNA accumulation are strictly controlled by RecA and likely correlate with intracellular iron levels. In addition, our study indicates that surface-associated growth of *S. oneidensis* MR-1 strongly requires a defense system against oxidative stress and tight control of iron uptake; however, levels of free intracellular iron and not hydrogen peroxide seem to limit induction and production of λSo on *S. oneidensis* MR-1 biofilms.

Alternative pathways for the induction of lambdoid phages that exclude the RecA-mediated SOS response have been identified (59, 60). In contrast, our results strongly suggest that induction of prophage λSo is strictly RecA dependent in *S. oneidensis* MR-1, both in planktonic cultures and in biofilms. Unexpectedly, Δ*recA* deletion mutants did not phenocopy Δλ*So* deletion mutants with regard to biofilm biomass and biofilm architecture. We hypothesize that this effect is due to secondary effects of the Δ*recA* mutation or due to the inability of Δ*recA* mutants to repair double-strand breaks. As previously suggested, cell death might therefore occur more often in Δ*recA* mutants during biofilm growth, resulting in *S. oneidensis* biofilms in the release of biofilm-promoting factors, which might partially complement the loss of λSo prophage-induced lysis (61).

We demonstrated that λSo induction is restricted mainly to filamentous cells, a commonly occurring but so far uncharacterized phenotypic variant in *S. oneidensis* MR-1 biofilms, indicating that these cells suffer from increased levels of DNA damage, the activating signal for RecA. Elongated cell morphologies in response to DNA damage had already been observed by Gates in the early 1930s (62). Later, they were shown to be a consequence of cell division inhibition while cellular growth proceeds, a process that is predominantly regulated by the RecA-mediated SOS response. In addition to gaining time for DNA repair, filamentation can also represent a fitness advantage in stressful environments (for a review, see reference 63). Notably, the occurrence of filamentous cells appears to be a rather common but so far not well understood phenomenon in microbial biofilms. In *Pseudomonas aeruginosa* biofilms, cell elongation correlates with nutrient deprivation under aerobic conditions and is triggered by nitric oxide production during anaerobic respiration (64, 65), two processes that might increase DNA damage. Analogously, formation of knitted chains in *Listeria monocytogenes* biofilms is controlled by SOS response factor YneA in response to oxidative stress (66, 67). Filamentous cells were also observed in environmental biofilm communities attached to microbial fuel cells, indicating that elongated cell morphologies might play a role in naturally occurring mixed electrogenic communities (68). Correspondingly, artificially induced elongation of *S. oneidensis* MR-1 cells was shown to enhance microbe-electrode interactions in microbial fuel cells (69). However, it is still unclear whether filamentous growth itself is required for normal biofilm formation of *S. oneidensis* MR-1 or whether it occurs as a side effect of the SOS response prior to λSo-induced lysis and eDNA release.

We observed that induction of prophage λSo and eDNA accumulation correlated with levels of ferrous iron. We primarily utilized ferrous iron throughout this study; however, spontaneous oxidation will have produced significant fractions of ferric iron during the experiments, and thus a clear distinction between the effects of the two forms was not possible.

Iron is present in most living organisms, in which it plays important roles in key enzymatic reactions, and has been shown to affect biofilms of multiple bacterial species. However, the exact regulatory pathways and physiological roles of iron during biofilm formation remain mostly unknown and likely vary among the species. Iron limitation has been demonstrated to induce biofilm formation in *Legionella pneumophila*, *Staphylococcus aureus*, and *Streptococcus mutans* (70–72) but inhibits this process in *E. coli*, *Vibrio cholerae*, and *P. aeruginosa* (73–75). High levels of iron disrupt *P. aeruginosa* biofilms, indicating that the effect occurs in a concentration-dependent fashion (76, 77). A recent study provides evidence that iron is implicated in the formation of *S. oneidensis* MR-1 pellicles (78). Generally, differential responses to iron levels may be a consequence of the organism's metabolic requirements, including the repertoire of iron metalloenzymes involved in specific metabolic pathways (73).

S. oneidensis MR-1 is capable of utilizing multiple organic and inorganic alternative terminal electron acceptors, and for this respiratory versatility *S. oneidensis* MR-1 requires a large array of iron-containing cytochromes (79). Thus, the ability to grow on diverse redox-active surfaces might account for a high demand for iron. In a recent study, we observed the induction of genes involved in iron uptake in response to early surface-associated growth (48). Accordingly, increased intracellular levels of free iron might generate DNA damage that ultimately induces λSo prophage induction. Expression profiles of *Salmonella enterica* serovar Typhimurium suggest that the lag phase similarly involves transient accumulation of iron and oxidative stress (80). Cells in lag phase might therefore adapt their physiological status to new environmental conditions in a way similar to the response of cells during early surface contact. To gain more insights into the course of iron uptake during biofilm formation, we generated an episomal promoter fusion of the putative *tonB* (SO_3670) promoter and *venus* (see Fig. S8B in the supplemental material). Promoter activities as indicated by fluorescence were highest during the

early phases of biofilm formation, suggesting that ferric iron uptake is repressed at later stages, potentially to control iron-induced oxidative damage. Accordingly, the level of λSo prophage induction decreases in later phases of biofilm development.

When *S. oneidensis* MR-1 attaches to mineral surfaces, reduction and solubilization of metal oxides likely result in locally increased ferrous iron concentrations (81). This would be expected to enhance λSo prophage induction and eDNA accumulation, as has been observed in the presence of additional ferrous iron in flow chamber biofilms in this study. Accordingly, genes belonging to prophage λSo were found to be induced during growth of *S. oneidensis* MR-1 on Fe nanoparticle-decorated anodes in microbial electrolysis cells, indicative of λSo prophage-mediated cell lysis (82).

Accumulation of eDNA during biofilm development might have beneficial effects in limiting λSo prophage induction by chelation of free iron in later phases (14). Oxygen and nutrient levels decrease within the depth of the biofilm; accordingly, λSo prophage induction and eDNA accumulation were observed to occur mainly in upper biofilm layers. In filamentous cells, the nutrient collection surface is enlarged while the surface-to-volume ratio remains similar (64). Hence, filamentous growth itself might indirectly contribute to an increase in intracellular iron levels in a positive-feedback loop, thereby triggering DNA damage and further filamentous growth. Furthermore, iron-induced DNA damage might be enhanced by the release of additional iron from iron-sulfur clusters that were damaged by oxidative stress (83). Hence, these two processes might in part elicit the observed heterogeneity in *S. oneidensis* MR-1 biofilms.

Similar to Δ*fur*, deletion of *oxyR* resulted in an increase in λSo prophage induction during biofilm formation, indicating that the OxyR-mediated response is involved, to some extent, in protecting biofilm cells against oxidative stress. It should be noted that the *fur* gene often belongs to the OxyR regulon (54). However, quantitative real-time RT-PCR analyses indicated that this is not the case in *S. oneidensis* MR-1. To explore the role of Fenton chemistry in the induction of λSo under biofilm conditions, we screened for mutations that trigger OxyR constitutively active to suppress H_2O_2-mediated induction of λSo, and we successfully isolated two mutants, $OxyR^{T104N}$ and $OxyR^{L197P}$. Notably, the OxyR threonine residue at position 104 is highly conserved among proteobacteria and seems to represent a functional "on-switch" of OxyR by replacement by asparagine (see Fig. S5A in the supplemental material). Thus, we propose that substitution T104N may also be broadly applied for OxyR research in further studies.

In contrast to the general assumption that DNA lesions in the presence of ferrous iron are the result of Fenton-generated (hydroxyl) radicals, our data indicate that iron and not H_2O_2 levels appear to be limiting for prophage λSo induction in biofilms, since the level of λSo induction was unaffected in biofilms formed by the H_2O_2-resistant OxyR mutants ($OxyR^{T104N}$ and $OxyR^{L197P}$). Previously, Flemmig and Arnhold observed Fe^{2+}-induced DNA strand breaks in plasmid pBBR322 that were not mediated by H_2O_2 (84). Further, it has been suggested earlier that oxidation of biomolecules by ferrous iron and dioxygen without participation of H_2O_2 is more relevant under physiological conditions than oxidation by hydroxyl radicals generated by Fenton chemistry. A study of Fenton-mediated radical oxidations of biomolecules to those induced by iron-oxygen complexes strongly indicated that at physiological ratios of $[O_2]/[H_2O_2]$, which range between 10^3 and 10^5, detrimental effects of iron-oxygen complexes become predominant over Fenton-derived radicals (85). Accordingly, the presence of free iron and dioxygen was assumed to be sufficient for damaging biomolecules such as DNA (84–86). Thus, based on these and our observations, we hypothesize that elevated iron uptake in the presence of oxygen might result in DNA damage without significant participation of Fenton chemistry, and ultimately in RecA-mediated λSo prophage induction and cell lysis in the upper layers of *S. oneidensis* MR-1 biofilms. However, further studies focusing on the effects of iron on the integrity chromosomal DNA in biofilm cells are required to explore the exact radical chemistry that might indirectly trigger λSo induction.

Notably, biofilm conditions have been reported to promote DNA double-strand breaks in various Gram-negative and Gram-positive species, generating genetic diversity that may help the community to adapt to varying environmental conditions or to generate antibiotic resistance (61, 66, 67, 87, 88). In these studies, the authors suggest oxidative stress to be responsible for the emergence of DNA lesions by a yet-unknown mechanism. Based on our observations, we hypothesize that intracellular iron levels might play a central role in these processes. Possibly, Fenton-independent iron-induced radical oxidation reactions may be a ubiquitous phenomenon with a so far underestimated and/or overlooked impact on microbial physiology and ecology. Our present study gives an example of the elaborate interplay between cellular requirements for iron, iron-induced DNA damage, prophage-induced lysis, and eDNA release during biofilm formation, which we expect to be similarly relevant for other bacterial species.

ACKNOWLEDGMENTS

This work was supported by the Max-Planck-Gesellschaft and the International Max Planck Research School for Environmental, Cellular and Molecular Microbiology (IMPRS-MIC) at the MPI für terrestrische Mikrobiologie.

REFERENCES

1. **Costerton JW.** 1995. Overview of microbial biofilms. J. Ind. Microbiol. **15:**137–140. http://dx.doi.org/10.1007/BF01569816.
2. **Hall-Stoodley L, Costerton JW, Stoodley P.** 2004. Bacterial biofilms: from the natural environment to infectious diseases. Nat. Rev. Microbiol. **2:**95–108. http://dx.doi.org/10.1038/nrmicro821.
3. **Flemming HC, Wingender J.** 2010. The biofilm matrix. Nat. Rev. Microbiol. **8:**623–633.
4. **Whitchurch CB, Tolker-Nielsen T, Ragas PC, Mattick JS.** 2002. Extracellular DNA required for bacterial biofilm formation. Science **295:**1487. http://dx.doi.org/10.1126/science.295.5559.1487.
5. **Rice KC, Mann EE, Endres JL, Weiss EC, Cassat JE, Smeltzer MS, Bayles KW.** 2007. The cidA murein hydrolase regulator contributes to DNA release and biofilm development in *Staphylococcus aureus*. Proc. Natl. Acad. Sci. U. S. A. **104:**8113–8118. http://dx.doi.org/10.1073/pnas.0610226104.
6. **Thomas VC, Thurlow LR, Boyle D, Hancock LE.** 2008. Regulation of autolysis-dependent extracellular DNA release by *Enterococcus faecalis* extracellular proteases influences biofilm development. J. Bacteriol. **190:**5690–5698. http://dx.doi.org/10.1128/JB.00314-08.
7. **Das T, Sharma PK, Busscher HJ, van der Mei HC, Krom BP.** 2010. Role of extracellular DNA in initial bacterial adhesion and surface aggregation. Appl. Environ. Microbiol. **76:**3405–3408. http://dx.doi.org/10.1128/AEM.03119-09.
8. **Steichen CT, Cho C, Shao JQ, Apicella MA.** 2011. The *Neisseria gonorrhoeae* biofilm matrix contains DNA, and an endogenous nuclease controls its incorporation. Infect. Immun. **79:**1504–1511. http://dx.doi.org/10.1128/IAI.01162-10.
9. **Gödeke J, Paul K, Lassak J, Thormann KM.** 2011. Phage-induced lysis enhances biofilm formation in *Shewanella oneidensis* MR-1. ISME J. **5:**613–626. http://dx.doi.org/10.1038/ismej.2010.153.

10. **Vilain S, Pretorius JM, Theron J, Brozel VS.** 2009. DNA as an adhesin: *Bacillus cereus* requires extracellular DNA to form biofilms. Appl. Environ. Microbiol. **75:**2861–2868. http://dx.doi.org/10.1128/AEM.01317-08.
11. **Pinchuk GE, Ammons C, Culley DE, Li SM, McLean JS, Romine MF, Nealson KH, Fredrickson JK, Beliaev AS.** 2008. Utilization of DNA as a sole source of phosphorus, carbon, and energy by *Shewanella* spp.: ecological and physiological implications for dissimilatory metal reduction. Appl. Environ. Microbiol. **74:**1198–1208. http://dx.doi.org/10.1128/AEM.02026-07.
12. **Heun M, Binnenkade L, Kreienbaum M, Thormann KM.** 2012. Functional specificity of extracellular nucleases of *Shewanella oneidensis* MR-1. Appl. Environ. Microbiol. **78:**4400–4411. http://dx.doi.org/10.1128/AEM.07895-11.
13. **Molin S, Tolker-Nielsen T.** 2003. Gene transfer occurs with enhanced efficiency in biofilms and induces enhanced stabilisation of the biofilm structure. Curr. Opin. Biotechnol. **14:**255–261. http://dx.doi.org/10.1016/S0958-1669(03)00036-3.
14. **Mulcahy H, Charron-Mazenod L, Lewenza S.** 2008. Extracellular DNA chelates cations and induces antibiotic resistance in *Pseudomonas aeruginosa* biofilms. PLoS Pathog. **4:**e1000213. http://dx.doi.org/10.1371/journal.ppat.1000213.
15. **Lewenza S.** 2013. Extracellular DNA-induced antimicrobial peptide resistance mechanisms in *Pseudomonas aeruginosa*. Front. Microbiol. **4:**21. http://dx.doi.org/10.3389/fmicb.2013.00021.
16. **Gloag ES, Turnbull L, Huang A, Vallotton P, Wang H, Nolan LM, Mililli L, Hunt C, Lu J, Osvath SR, Monahan LG, Cavaliere R, Charles IG, Wand MP, Gee ML, Prabhakar R, Whitchurch CB.** 2013. Self-organization of bacterial biofilms is facilitated by extracellular DNA. Proc. Natl. Acad. Sci. U. S. A. **110:**11541–11546. http://dx.doi.org/10.1073/pnas.1218898110.
17. **Allesen-Holm M, Barken KB, Yang L, Klausen M, Webb JS, Kjelleberg S, Molin S, Givskov M, Tolker-Nielsen T.** 2006. A characterization of DNA release in *Pseudomonas aeruginosa* cultures and biofilms. Mol. Microbiol. **59:**1114–1128. http://dx.doi.org/10.1111/j.1365-2958.2005.05008.x.
18. **Sahu PK, Iyer PS, Oak AM, Pardesi KR, Chopade BA.** 2012. Characterization of eDNA from the clinical strain *Acinetobacter baumannii* AIIMS 7 and its role in biofilm formation. ScientificWorldJournal **2012:** 973436. http://dx.doi.org/10.1100/2012/973436.
19. **Hamilton HL, Dominguez NM, Schwartz KJ, Hackett KT, Dillard JP.** 2005. *Neisseria gonorrhoeae* secretes chromosomal DNA via a novel type IV secretion system. Mol. Microbiol. **55:**1704–1721. http://dx.doi.org/10.1111/j.1365-2958.2005.04521.x.
20. **Barnes AM, Ballering KS, Leibman RS, Wells CL, Dunny GM.** 2012. *Enterococcus faecalis* produces abundant extracellular structures containing DNA in the absence of cell lysis during early biofilm formation. mBio **3:**e00193–12. http://dx.doi.org/10.1128/mBio.00193-12.
21. **Zweig MA, Schork S, Koerdt A, Siewering K, Sternberg C, Thormann K, Albers SV, Molin S, van der Does C.** 2013. Secreted single-stranded DNA is involved in the initial phase of biofilm formation by *Neisseria gonorrhoeae*. Environ. Microbiol. **16:**1040–1052. http://dx.doi.org/10.1111/1462-2920.12291.
22. **Lappann M, Claus H, van Alen T, Harmsen M, Elias J, Molin S, Vogel U.** 2010. A dual role of extracellular DNA during biofilm formation of *Neisseria meningitidis*. Mol. Microbiol. **75:**1355–1371. http://dx.doi.org/10.1111/j.1365-2958.2010.07054.x.
23. **Zhao J, Wang Q, Li M, Heijstra BD, Wang S, Liang Q, Qi Q.** 2013. *Escherichia coli* toxin gene hipA affects biofilm formation and DNA release. Microbiology **159:**633–640. http://dx.doi.org/10.1099/mic.0.063784-0.
24. **Paul JH.** 2008. Prophages in marine bacteria: dangerous molecular time bombs or the key to survival in the seas? ISME J. **2:**579–589. http://dx.doi.org/10.1038/ismej.2008.35.
25. **Wang X, Kim Y, Ma Q, Hong SH, Pokusaeva K, Sturino JM, Wood TK.** 2010. Cryptic prophages help bacteria cope with adverse environments. Nat. Commun. **1:**147. http://dx.doi.org/10.1038/ncomms1146.
26. **Fortier LC, Sekulovic O.** 2013. Importance of prophages to evolution and virulence of bacterial pathogens. Virulence **4:**354–365. http://dx.doi.org/10.4161/viru.24498.
27. **Hong SH, Wang X, Wood TK.** 2010. Controlling biofilm formation, prophage excision and cell death by rewiring global regulator H-NS of *Escherichia coli*. Microb. Biotechnol. **3:**344–356. http://dx.doi.org/10.1111/j.1751-7915.2010.00164.x.
28. **Rice SA, Tan CH, Mikkelsen PJ, Kung V, Woo J, Tay M, Hauser A, McDougald D, Webb JS, Kjelleberg S.** 2009. The biofilm life cycle and virulence of *Pseudomonas aeruginosa* are dependent on a filamentous prophage. ISME J. **3:**271–282. http://dx.doi.org/10.1038/ismej.2008.109.
29. **Resch A, Fehrenbacher B, Eisele K, Schaller M, Gotz F.** 2005. Phage release from biofilm and planktonic *Staphylococcus aureus* cells. FEMS Microbiol. Lett. **252:**89–96. http://dx.doi.org/10.1016/j.femsle.2005.08.048.
30. **Wang X, Kim Y, Wood TK.** 2009. Control and benefits of CP4-57 prophage excision in *Escherichia coli* biofilms. ISME J. **3:**1164–1179. http://dx.doi.org/10.1038/ismej.2009.59.
31. **Webb JS, Thompson LS, James S, Charlton T, Tolker-Nielsen T, Koch B, Givskov M, Kjelleberg S.** 2003. Cell death in *Pseudomonas aeruginosa* biofilm development. J. Bacteriol. **185:**4585–4592. http://dx.doi.org/10.1128/JB.185.15.4585-4592.2003.
32. **Petrova OE, Schurr JR, Schurr MJ, Sauer K.** 2011. The novel *Pseudomonas aeruginosa* two-component regulator BfmR controls bacteriophage-mediated lysis and DNA release during biofilm development through PhdA. Mol. Microbiol. **81:**767–783. http://dx.doi.org/10.1111/j.1365-2958.2011.07733.x.
33. **Carrolo M, Frias MJ, Pinto FR, Melo-Cristino J, Ramirez M.** 2010. Prophage spontaneous activation promotes DNA release enhancing biofilm formation in *Streptococcus pneumoniae*. PLoS One **5:**e15678. http://dx.doi.org/10.1371/journal.pone.0015678.
34. **Jiang SC, Kellogg CA, Paul JH.** 1998. Characterization of marine temperate phage-host systems isolated from Mamala Bay, Oahu, Hawaii. Appl. Environ. Microbiol. **64:**535–542.
35. **Jiang SC, Paul JH.** 1994. Seasonal and diel abundance of viruses and occurrence of lysogeny/bacteriocinogeny in the marine-environment. Mar. Ecol. Prog. Ser. **104:**163–172. http://dx.doi.org/10.3354/meps104163.
36. **Stopar D, Cerne A, Zigman M, Poljsak-Prijatelj M, Turk V.** 2004. Viral abundance and a high proportion of lysogens suggest that viruses are important members of the microbial community in the Gulf of Trieste. Microb. Ecol. **47:**1–8. http://dx.doi.org/10.1007/s00248-002-3009-5.
37. **Leitet C, Riemann L, Hagstrom A.** 2006. Plasmids and prophages in Baltic Sea bacterioplankton isolates. J. Mar. Biol. Assoc. UK **86:**567–575. http://dx.doi.org/10.1017/S0025315406013488.
38. **Ptashne M.** 2004. A genetic switch: phage lambda revisited, vol 3. Cold Spring Harbor Laboratory Press, Cold Spring Harbor, NY.
39. **Qiu X, Sundin GW, Wu L, Zhou J, Tiedje JM.** 2005. Comparative analysis of differentially expressed genes in *Shewanella oneidensis* MR-1 following exposure to UVC, UVB, and UVA radiation. J. Bacteriol. **187:** 3556–3564. http://dx.doi.org/10.1128/JB.187.10.3556-3564.2005.
40. **Bus JS, Gibson JE.** 1984. Paraquat: model for oxidant-initiated toxicity. Environ. Health Perspect. **55:**37–46. http://dx.doi.org/10.1289/ehp.845537.
41. **Sambrook J, Fritsch E, Maniatis T.** 1989. Molecular cloning: a laboratory manual. Cold Spring Harbor Laboratory Press, Cold Spring Harbor, NY.
42. **Lassak J, Henche AL, Binnenkade L, Thormann KM.** 2010. ArcS, the cognate sensor kinase in an atypical Arc system of *Shewanella oneidensis* MR-1. Appl. Environ. Microbiol. **76:**3263–3274. http://dx.doi.org/10.1128/AEM.00512-10.
43. **Aiba H, Adhya S, de Crombrugghe B.** 1981. Evidence for two functional *gal* promoters in intact *Escherichia coli* cells. J. Biol. Chem. **256:**11905–11910.
44. **Pfaffl MW.** 2001. A new mathematical model for relative quantification in real-time RT-PCR. Nucleic Acids Res. **29:**e45. http://dx.doi.org/10.1093/nar/29.9.e45.
45. **Steinmoen H, Knutsen E, Havarstein LS.** 2002. Induction of natural competence in *Streptococcus pneumoniae* triggers lysis and DNA release from a subfraction of the cell population. Proc. Natl. Acad. Sci. U. S. A. **99:**7681–7686. http://dx.doi.org/10.1073/pnas.112464599.
46. **Miller JH.** 1972. A short course in bacterial genetics. Cold Spring Harbor Laboratory Press, Cold Spring Harbor, NY.
47. **Thormann KM, Saville RM, Shukla S, Pelletier DA, Spormann AM.** 2004. Initial phases of biofilm formation in *Shewanella oneidensis* MR-1. J. Bacteriol. **186:**8096–8104. http://dx.doi.org/10.1128/JB.186.23.8096-8104.2004.
48. **Gödeke J, Binnenkade L, Thormann KM.** 2012. Transcriptome analysis of early surface-associated growth of *Shewanella oneidensis* MR-1. PLoS One **7:**e42160. http://dx.doi.org/10.1371/journal.pone.0042160.
49. **Fuangthong M, Mongkolsuk S.** 1997. Isolation and characterization of a multiple peroxide resistant mutant from *Xanthomonas campestris* pv. *phaseoli*. FEMS Microbiol. Lett. **152:**189–194. http://dx.doi.org/10.1111/j.1574-6968.1997.tb10427.x.

50. **Mongkolsuk S, Whangsuk W, Fuangthong M, Loprasert S.** 2000. Mutations in *oxyR* resulting in peroxide resistance in *Xanthomonas campestris*. J. Bacteriol. **182:**3846–3849. http://dx.doi.org/10.1128/JB.182.13.3846-3849.2000.
51. **Jiang Y, Dong Y, Luo Q, Li N, Wu G, Gao H.** 2014. Protection from oxidative stress relies mainly on derepression of OxyR-dependent KatB and Dps in *Shewanella oneidensis*. J. Bacteriol. **196:**445–458. http://dx.doi.org/10.1128/JB.01077-13.
52. **Wan XF, Verberkmoes NC, McCue LA, Stanek D, Connelly H, Hauser LJ, Wu L, Liu X, Yan T, Leaphart A, Hettich RL, Zhou J, Thompson DK.** 2004. Transcriptomic and proteomic characterization of the Fur modulon in the metal-reducing bacterium *Shewanella oneidensis*. J. Bacteriol. **186:**8385–8400. http://dx.doi.org/10.1128/JB.186.24.8385-8400.2004.
53. **Schlacher K, Goodman MF.** 2007. Lessons from 50 years of SOS DNA-damage-induced mutagenesis. Nat. Rev. Mol. Cell Biol. **8:**587–594. http://dx.doi.org/10.1038/nrm2198.
54. **Cornelis P, Wei Q, Andrews SC, Vinckx T.** 2011. Iron homeostasis and management of oxidative stress response in bacteria. Metallomics **3:**540–549. http://dx.doi.org/10.1039/c1mt00022e.
55. **Imlay JA.** 2013. The molecular mechanisms and physiological consequences of oxidative stress: lessons from a model bacterium. Nat. Rev. Microbiol. **11:**443–454. http://dx.doi.org/10.1038/nrmicro3032.
56. **Goodwin JF, Whitten CF.** 1965. Chelation of ferrous sulphate solutions by desferrioxamine B. Nature **205:**281–283. http://dx.doi.org/10.1038/205281b0.
57. **Grant RA, Filman DJ, Finkel SE, Kolter R, Hogle JM.** 1998. The crystal structure of Dps, a ferritin homolog that binds and protects DNA. Nat. Struct. Biol. **5:**294–303. http://dx.doi.org/10.1038/nsb0498-294.
58. **Almiron M, Link AJ, Furlong D, Kolter R.** 1992. A novel DNA-binding protein with regulatory and protective roles in starved *Escherichia coli*. Genes Dev. **6:**2646–2654. http://dx.doi.org/10.1101/gad.6.12b.2646.
59. **Rozanov DV, D'Ari R, Sineoky SP.** 1998. RecA-independent pathways of lambdoid prophage induction in *Escherichia coli*. J. Bacteriol. **180:**6306–6315.
60. **Ghosh D, Roy K, Williamson KE, Srinivasiah S, Wommack KE, Radosevich M.** 2009. Acyl-homoserine lactones can induce virus production in lysogenic bacteria: an alternative paradigm for prophage induction. Appl. Environ. Microbiol. **75:**7142–7152. http://dx.doi.org/10.1128/AEM.00950-09.
61. **Boles BR, Singh PK.** 2008. Endogenous oxidative stress produces diversity and adaptability in biofilm communities. Proc. Natl. Acad. Sci. U. S. A. **105:**12503–12508. http://dx.doi.org/10.1073/pnas.0801499105.
62. **Gates FL.** 1933. The reaction of individual bacteria to irradiation with ultraviolet light. Science **77:**350. http://dx.doi.org/10.1126/science.77.1997.350.
63. **Justice SS, Hunstad DA, Cegelski L, Hultgren SJ.** 2008. Morphological plasticity as a bacterial survival strategy. Nat. Rev. Microbiol. **6:**162–168. http://dx.doi.org/10.1038/nrmicro1820.
64. **Steinberger RE, Allen AR, Hansma HG, Holden PA.** 2002. Elongation correlates with nutrient deprivation in *Pseudomonas aeruginosa*-unsaturated biofilms. Microb. Ecol. **43:**416–423. http://dx.doi.org/10.1007/s00248-001-1063-z.
65. **Yoon MY, Lee KM, Park Y, Yoon SS.** 2011. Contribution of cell elongation to the biofilm formation of *Pseudomonas aeruginosa* during anaerobic respiration. PLoS One **6:**e16105. http://dx.doi.org/10.1371/journal.pone.0016105.
66. **van der Veen S, Abee T.** 2011. Generation of variants in *Listeria monocytogenes* continuous-flow biofilms is dependent on radical-induced DNA damage and RecA-mediated repair. PLoS One **6:**e28590. http://dx.doi.org/10.1371/journal.pone.0028590.
67. **van der Veen S, Abee T.** 2010. Dependence of continuous-flow biofilm formation by *Listeria monocytogenes* EGD-e on SOS response factor YneA. Appl. Environ. Microbiol. **76:**1992–1995. http://dx.doi.org/10.1128/AEM.02680-09.
68. **Ishii S, Shimoyama T, Hotta Y, Watanabe K.** 2008. Characterization of a filamentous biofilm community established in a cellulose-fed microbial fuel cell. BMC Microbiol. **8:**6. http://dx.doi.org/10.1186/1471-2180-8-6.
69. **Patil SA, Gorecki K, Hagerhall C, Gorton L.** 2013. Cisplatin-induced elongation of *Shewanella oneidensis* MR-1 cells improves microbe-electrode interactions for use in microbial fuel cells. Energ. Environ. Sci. **6:**2626–2630. http://dx.doi.org/10.1039/c3ee41974f.
70. **Berlutti F, Ajello M, Bosso P, Morea C, Petrucca A, Antonini G, Valenti P.** 2004. Both lactoferrin and iron influence aggregation and biofilm formation in *Streptococcus mutans*. Biometals **17:**271–278. http://dx.doi.org/10.1023/B:BIOM.0000027704.53859.d3.
71. **Johnson M, Cockayne A, Williams PH, Morrissey JA.** 2005. Iron-responsive regulation of biofilm formation in *Staphylococcus aureus* involves fur-dependent and fur-independent mechanisms. J. Bacteriol. **187:**8211–8215. http://dx.doi.org/10.1128/JB.187.23.8211-8215.2005.
72. **Hindre T, Bruggemann H, Buchrieser C, Hechard Y.** 2008. Transcriptional profiling of *Legionella pneumophila* biofilm cells and the influence of iron on biofilm formation. Microbiology **154:**30–41. http://dx.doi.org/10.1099/mic.0.2007/008698-0.
73. **Wu Y, Outten FW.** 2009. IscR controls iron-dependent biofilm formation in *Escherichia coli* by regulating type I fimbria expression. J. Bacteriol. **191:**1248–1257. http://dx.doi.org/10.1128/JB.01086-08.
74. **Banin E, Brady KM, Greenberg EP.** 2006. Chelator-induced dispersal and killing of *Pseudomonas aeruginosa* cells in a biofilm. Appl. Environ. Microbiol. **72:**2064–2069. http://dx.doi.org/10.1128/AEM.72.3.2064-2069.2006.
75. **Banin E, Vasil ML, Greenberg EP.** 2005. Iron and *Pseudomonas aeruginosa* biofilm formation. Proc. Natl. Acad. Sci. U. S. A. **102:**11076–11081. http://dx.doi.org/10.1073/pnas.0504266102.
76. **Musk DJ, Banko DA, Hergenrother PJ.** 2005. Iron salts perturb biofilm formation and disrupt existing biofilms of *Pseudomonas aeruginosa*. Chem. Biol. **12:**789–796. http://dx.doi.org/10.1016/j.chembiol.2005.05.007.
77. **Yang L, Barken KB, Skindersoe ME, Christensen AB, Givskov M, Tolker-Nielsen T.** 2007. Effects of iron on DNA release and biofilm development by *Pseudomonas aeruginosa*. Microbiology **153:**1318–1328. http://dx.doi.org/10.1099/mic.0.2006/004911-0.
78. **Yuan J, Chen Y, Zhou G, Chen H, Gao H.** 2013. Investigation of roles of divalent cations in *Shewanella oneidensis* pellicle formation reveals unique impacts of insoluble iron. Biochim. Biophys. Acta **1830:**5248–5257. http://dx.doi.org/10.1016/j.bbagen.2013.07.023.
79. **Meyer TE, Tsapin AI, Vandenberghe I, de Smet L, Frishman D, Nealson KH, Cusanovich MA, van Beeumen JJ.** 2004. Identification of 42 possible cytochrome C genes in the *Shewanella oneidensis* genome and characterization of six soluble cytochromes. OMICS **8:**57–77. http://dx.doi.org/10.1089/153623104773547499.
80. **Rolfe MD, Rice CJ, Lucchini S, Pin C, Thompson A, Cameron ADS, Alston M, Stringer MF, Betts RP, Baranyi J, Peck MW, Hinton JCD.** 2012. Lag phase is a distinct growth phase that prepares bacteria for exponential growth and involves transient metal accumulation. J. Bacteriol. **194:**686–701. http://dx.doi.org/10.1128/JB.06112-11.
81. **Lovley DR, Holmes DE, Nevin KP.** 2004. Dissimilatory Fe(III) and Mn(IV) reduction. Adv. Microb. Physiol. **49:**219–286. http://dx.doi.org/10.1016/S0065-2911(04)49005-5.
82. **Xu S, Liu H, Fan Y, Schaller R, Jiao J, Chaplen F.** 2012. Enhanced performance and mechanism study of microbial electrolysis cells using Fe nanoparticle-decorated anodes. Appl. Microbiol. Biotechnol. **93:**871–880. http://dx.doi.org/10.1007/s00253-011-3643-2.
83. **Jang S, Imlay JA.** 2007. Micromolar intracellular hydrogen peroxide disrupts metabolism by damaging iron-sulfur enzymes. J. Biol. Chem. **282:**929–937. http://dx.doi.org/10.1074/jbc.M607646200.
84. **Flemmig J, Arnhold J.** 2007. Ferrous ion-induced strand breaks in the DNA plasmid pBR322 are not mediated by hydrogen peroxide. Eur. Biophys. J. **36:**377–384. http://dx.doi.org/10.1007/s00249-006-0093-3.
85. **Qian SY, Buettner GR.** 1999. Iron and dioxygen chemistry is an important route to initiation of biological free radical oxidations: an electron paramagnetic resonance spin trapping study. Free Radic. Biol. Med. **26:**1447–1456. http://dx.doi.org/10.1016/S0891-5849(99)00002-7.
86. **Saran M, Michel C, Stettmaier K, Bors W.** 2000. Arguments against the significance of the Fenton reaction contributing to signal pathways under in vivo conditions. Free Radic. Res. **33:**567–579. http://dx.doi.org/10.1080/10715760000301101.
87. **Ryder VJ, Chopra I, O'Neill AJ.** 2012. Increased mutability of Staphylococci in biofilms as a consequence of oxidative stress. PLoS One **7:**e47695. http://dx.doi.org/10.1371/journal.pone.0047695.
88. **Driffield K, Miller K, Bostock JM, O'Neill AJ, Chopra I.** 2008. Increased mutability of *Pseudomonas aeruginosa* in biofilms. J. Antimicrob. Chemother. **61:**1053–1056. http://dx.doi.org/10.1093/jac/dkn044.